ChemSusChem

Chemistry–Sustainability–Energy–Materials

Chemistry Europe

European Chemical Societies Publishing

Accepted Article

Title: Recovery of Arenes from Polyethylene Terephthalate (PET) over a Co/TiO2 Catalyst

Authors: Surachet Hongkailers, Yaxuan Jing, Yanqin Wang, Napida Hinchiranan, and Ning Yan

To be cited as: *ChemSusChem* 10.1002/cssc.202100956

Link to VoR: https://doi.org/10.1002/cssc.202100956

WILEY-VCH

WILEY-VCH

FULL PAPER

Recovery of Arenes from Polyethylene Terephthalate (PET) over a Co/TiO_2 Catalyst

Surachet Hongkailers,[a,e] Yaxuan Jing,[b,e] Yanqin Wang,[b] Napida Hinchiranan,[a, c, d]* Ning Yan[e]*

[a] Surachet Hongkailers, Prof. Dr. Napida Hinchiranan
Department of Chemical Technology, Chulalongkorn University
254 Phyathai Road, Bangkok 10330, Thailand
E-mail: napida.h@chula.ac.th

[b] Dr. Yaxuan Jing, Prof. Dr. Yanqin Wang
Key Laboratory for Advanced Materials and Joint International Research Laboratory of Precision Chemistry and Molecular Engineering, Feringa Nobel Prize Scientist Joint Research Center, Research Institute of Industrial Catalysis, School of Chemistry and Molecular Engineering, East China University of Science and Technology, Shanghai 200237, China

[c] Prof. Dr. Napida Hinchiranan
Center of Excellence on Petrochemical and Materials Technology (PETROMAT), Chulalongkorn University
254 Phyathai Road, Bangkok 10330, Thailand

[d] Prof. Dr. Napida Hinchiranan
Center of Excellence in Catalysis for Bioenergy and Renewable Chemicals (CBRC), Chulalongkorn University
254 Phyathai Road, Bangkok 10330, Thailand

[e] Prof. Dr. Ning Yan
Department of Chemical and Biomolecular Engineering, National University of Singapore
4 Engineering Drive 4, Singapore 117585, Singapore
E-mail: ning.yan@nus.edu.sg

Supporting information for this article is given via a link at the end of the document.

Abstract: Upcycling of spent plastics becomes a more emergent topic than ever before due to the rapid generation of plastic waste associated with the change of lifestyles of the human society. Polyethylene terephthalate (PET) is a major aromatic plastic and herein, we demonstrate the conversion of PET back into arenes in a one-pot reaction combining depolymerization and hydrodeoxygenation (HDO) over a Co/TiO_2 catalyst. The effectiveness of the Co/TiO_2 catalyst in HDO and the underlining reaction pathway have been established using the PET monomer terephthalic acid (TPA) as the substrate. Quantitative TPA conversion together with 75.2 mol% xylene and toluene selectivity under 30 bar initial H_2 pressure at 340 °C was achieved after 4 h reaction. More encouragingly, the catalyst induced both depolymerization and HDO reaction via C-O bond cleavage when PET is used as a substrate. 78.9 mol% arenes (toluene and xylene) was obtained under optimized condition.

Introduction

Driven by the expansion of human population, as well as developments in economy and urbanization, plastic production and consumption are annually increased[1] from 279 million tons in 2011 to 368 million tons in 2019.[2] To make things worse, the lockdown and quarantine among the COVID-19 pandemic situation in 2020-2021 promote huge consumption of single-use plastic products for packaging and personal protection equipment, resulting in even larger amount of waste generation.[3] Due to the tardy degradation kinetics of plastics,[2a] they are accumulated on land or spread into the ocean, causing environmental problems to impact wildlife and human health.[4] The typical plastic waste management such as landfill and incineration are convenient for the treatment without sorting, but these disposals invade valuable land space and release toxic air pollutants.[5] Recycling, instead of landfills and incineration, is an alternative way to handle the problem, which better fits into the concept of circular economy,[6] and holds the potential to recover valuable chemicals from plastic wastes.[7]

Polyethylene terephthalate (PET), a synthetic aromatic polyester, is formed from terephthalic acid (TPA) and ethylene glycol.[8] Nowadays, PET becomes one of the most widely used commodity plastics in the world at an annual scale of about 50 million tons. Due to its thermal stability, chemical resistance, clarity, lightweight, as well as good tensile and impact strength, PET is widely used to manufacture beverage bottles, fibres, and filaments.[8-9] As with most other types of plastics, PET possesses a high resistance to biological degradation in nature, and consequently, efficient chemical approaches to degrade PET are under intensive development.[10] Existing methods involving hydrolysis,[11] glycolysis,[12] alcoholysis,[13] and reductive depolymerization are applied to produce TPA or bis(hydroxyethyl) terephthalate (BHET).[14] However, these route requires considerable amounts of solvents or depolymerizing agents (such as strong acid and base), imposing potential toxicity and ecological issues.[15] Pyrolysis, which has been very successful in treating polyethylene (PE), polypropylene (PP), polystyrene (PS)[5] and plastic mixtures,[2a, 5, 16] is not particularly effective in treating PET: a waxy-like product instead of liquid pyrolysis oil was generated under typical pyrolysis conditions.[17]

In industry, petroleum-derived arenes are used as the key starting material to produce PET. Converting PET back to aromatics and other hydrocarbons is an interesting strategy to decrease the reliance of these commodity chemicals on fossil resources.[18] Tang et al.[19] reported that 94.8% total yield of C_7-C_8 cycloalkanes and aromatics in the range of gasoline and jet fuel was produced from PET waste through alcoholysis, followed by hydrogenation and hydrodeoxygenation (HDO) over Pt/C and $Ru\text{-}Cu/SiO_2$ catalysts. The methanolysis of polycarbonate followed by HDO over Pt/C and HBeta zeolite was conducted to synthesize C_{13}-C_{15} polycycloalkanes as high-density aviation fuels.[20] Moreover, HDO of aromatic plastic wastes, including PET, polycarbonate, and polyphenylene oxide, have been

demonstrated over a Ru/Nb_2O_5 catalyst to access simple arenes.[21]

The HDO reaction has been extensively investigated in the past decade, in particular for upgrading biomass feedstock into low-oxygen products.[22] Noble-metal based catalysts, especially Pt-, Pd-, and Ru-containing ones,[23] exhibited excellent HDO activity in converting aromatic oxygenates [23a, 23d]. However, the high cost of these noble metals and their susceptibility to sulfur and nitrogen elements add barriers in practical uses. Metal sulfides and nitrides have also been reported to be moderately active,[24] but they suffer from the leaching of sulfur/nitrogen, which induces catalyst deactivation and product contamination.[24a] Thus, non-noble metal-based nanoparticle catalysts dispersed on metal oxide supports are attractive to treat aromatic oxygenates. At present, Ni[25] has been extensively studied in HOD reaction for biomass valorization, followed by Co[26]. Co catalysts display higher activity in HDO through C-O cleavage than Ni-based catalysts, the latter of which favor C-C bond breakage.[26c] Among various types of supports, titanium dioxide (TiO_2) showed good performance due to its defect sites for binding with oxygen atoms in the substrates,[27] the strong metal-support interaction and prevention of coke formation.[26b, 28]

Based on the analysis above, we prepared a Co/TiO_2 catalyst and tested its performance in PET conversion to arenes in the presence of hydrogen for the first time. Initially, HDO of terephthalic acid (TPA) was examined to study the reaction pathway and establish suitable reaction conditions. Following that the system was further extended to promote the upcycling of PET in a one pot manner, with satisfactory yields of arenes being obtained.

Results and Discussion

Catalyst characterization

The 5 wt% Co/TiO_2 catalyst was prepared via the wetness impregnation method using cobalt nitrate as the metal precursor and anatase as the support. The pre-catalyst was calcined at 500 °C and reduced under the H_2 atmosphere at 420 °C before reaction. The N_2 adsorption-desorption isotherms are shown in Figure 1a. Both the anatase support and the 5 wt% Co/TiO_2 catalyst showed IV-type isotherm typical for mesoporous materials (pore size 2-50 nm).[29] The isotherms also exhibited H3-type hysteresis loop, indicating the presence of macropores or aggregated plate-like particles.[29] The BET surface area, Barret-Joyner-Halenda (BJH) pore radius, and total pore volume of TiO_2 were 9.81 m^2/g, 1.92 nm, and 0.0156 cm^2/g (Table 1), respectively. These textural properties were similar both before and after Co loading, despite the values were slightly lower than that obtained from pure mesoporous TiO_2.[30]

Figure 1b shows the X-ray powder diffraction (XRD) patterns of TiO_2 and Co/TiO_2 catalysts in both calcined and reduced forms. A set of characteristic peaks at 25.3°, 36.9°, 37.8°, 38.5°, 48.1°, 53.9°, 55.1°, 62.1°, 62.7°, 68.8°, 70.2°, 75.0°, and 76.0 matched with the crystal planes (101), (103), (004), (112), (200), (105), (211), (213), (204), (116), (220), (215), and (301) of anatase TiO_2, respectively,.[30a] For the calcined Co/TiO_2 catalyst, additional diffraction peaks appeared at 31.3°, 44.8°, 59.5°, and 65.4° corresponding to Co_3O_4.[31] The peak at 44.3° assigned to metallic Co^0 was noticed for the reduced Co/TiO_2 catalyst.[26b] Of note, the XRD pattern of TiO_2 after calcination and reduction did not change, indicating that the thermal treatments were below the temperature required for the phase transformation of anatase to rutile, which typically started at 600 °C.[32] The presence of Co_3O_4 diffraction peaks in the XRD pattern of the calcined Co/TiO_2 catalyst implies successful deposition of Co on the TiO_2 support. Likewise, the appearance of the characteristic Co^0 peak after reduction confirms the existence of metallic Co phase after H_2 reduction.

According to the ICP-OES results, the precise amount of Co in the Co/TiO_2 catalyst was 4.92 wt% (Table 1), close to the targeted content of 5 wt%. Transmission electron microscopy (TEM) image (Figure 1c) revealed that the Co particles were deposited on the outer surface of the TiO_2 support. This is in line with the Co particle size estimated from XRD patterns using Scherrer's equation (19.1 nm, Table 1), which is too large to be located inside the TiO_2 pores. Similar phenomenon has been reported in some types of catalysts such as the silica fiber and silica ball supported metal catalysts.[30b, 33] The Co loading via impregnation method might be another factor for agglomerated Co particles. Interestingly, large molecules such as TPA and especially PET cannot easily diffuse into small pores of the catalyst support. Thus, the low surface area of TiO_2 bearing Co particles on the outer surface might be beneficial to conduct the HDO of TPA and PET. The dispersion of Co was estimated to be around 5% based on the particle size of Co.

The H_2-TPR profile and H_2 consumption of the Co/TiO_2 catalyst are presented in Figure 1d and Table 2, respectively. The reduction of TiO_2 was also attested. There was no H_2 consumption over TiO_2, suggesting that the pure support was not reduced under H_2 atmosphere without Co. The H_2-TPR profile of Co/TiO_2 catalyst was deconvoluted into four peaks maximized at 380, 401, 480, and 753 °C, respectively. The lowest reduction temperature region plausibly corresponded to the reduction of Co_3O_4 (Co^{3+}) to CoO (Co^{2+}), while the following reduction zone was attributed to the reduction of CoO to Co^0.[26a] The third and the fourth peaks at comparatively higher reduction temperatures were also observed, likely due to the reduction of $CoTiO_3$ as reported previously.[26a, 34]

The acidity of TiO_2 and calcined Co/TiO_2 catalyst was determined by NH_3-TPD analysis. The NH_3 desorption profiles were depicted in Figure S1 and the amount of desorbed NH_3 of each sample was shown in Table 2. The amount of desorbed NH_3 from weak, medium, and strong acid sites on TiO_2 was 29, 6, and 4 μmol NH_3/g, exhibiting that the weak acid sites were dominated on this support. For the Co/TiO_2 catalyst, more NH_3 desorption was observed for all types of acid sites, resulting in 64% higher total acidity than TiO_2. The increase in the acidity might be attributed to the Co oxide on the Co/TiO_2 catalyst. Azzi et al.[35] found that mesoporous Co_3O_4 catalyst had both Lewis and Bronsted acid sites via pyridine FT-IR technique.

Hydrodeoxygenation of TPA

TPA was applied as a model compound to verify whether the Co/TiO_2 catalyst is active in HDO of carboxylic acid at elevated temperatures under H_2. The products were analyzed by gas chromatography-mass spectrometry (GC-MS), with representative GC-MS chromatogram presented in Figure S2. A range of arene products were identified, which could be classified into two groups including hydrocarbons (e.g., xylene, toluene) and oxygenated arenes (e.g., 4-methylbenzyl alcohol and 4-methylbenzoic acid, including the coupling product (4-

methylphenol)methyl 4-methylbenzoate). The conversion of TPA and the yield of each product as a function of time, temperature, and initial H_2 pressure were shown in Figure 2. The product yields were quantified using calibration data obtained from GC-FID as shown in Table S1. The univariate experiment with central condition under 30 bar H_2 pressure at 300 °C for 4 h was used to study the effect of isolated parameters.

As shown in Figure 2a, increase in the reaction time from 2 to 8 h significantly enhanced the degree of TPA conversion from 37.9 to 70.0%, together with increased total product yield. In terms of selectivity, longer reaction time provided remarkably higher amounts of xylene and 4-methylbenzoic acid in the products, suggesting relatively high stability of these compounds. Moreover, the mole ratio of xylene/4-methylbenzoic acid increased from 0.35 to 0.93 with higher TPA conversion, implying that TPA may be firstly transformed into 4-methylbenzoic acid, which was subsequently converted to xylene.

Table 1. Textural properties, Co crystallite size and degree of Co dispersion of the Co/TiO_2 catalyst.

Sample	Co amount[a] (wt %)	S_{BET}[b] ($m^2\ g^{-1}$)	r_p[c] (nm)	V_p[d] ($cm^3\ g^{-1}$)	Co crystallite size[e] (nm)	Co dispersion[f] (%)
TiO_2	-	9.81	1.92	0.0156	-	-
Co/TiO_2	4.92	10.38	1.54	0.0173	19.1	5.02

[a] Analyzed from ICP-OES technique. [b] S_{BET} = BET Surface Area. [c] r_p = BJH pore radius. [d] V_p = total pore volume. [e] Estimated from the widths of XRD peaks using Scherrer's equation (2θ = 44.3°).[26a] [f] Calculated from Co dispersion (%) = 96/Co crystallite size (nm).[26a]

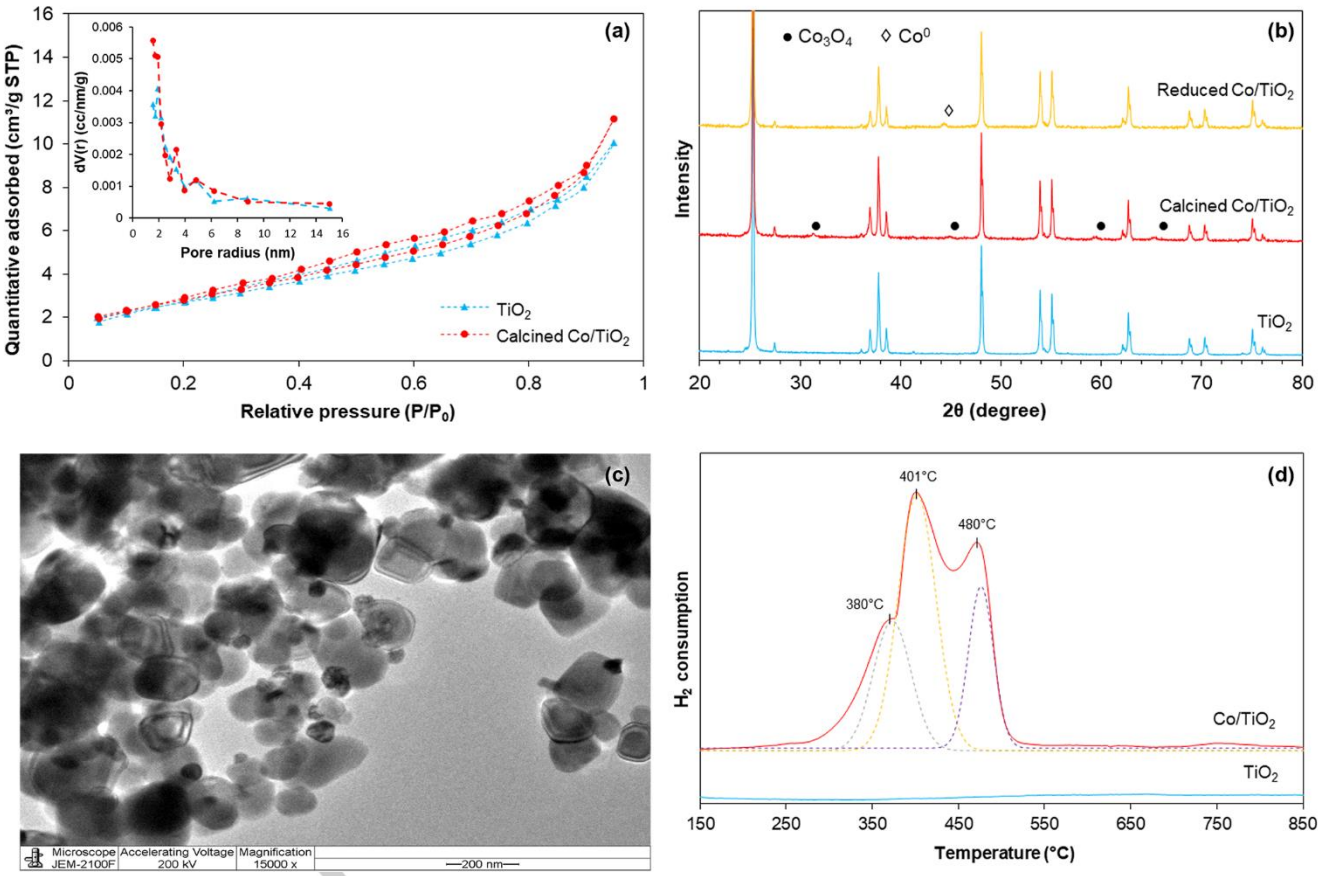

Figure 1. (a) N_2 adsorption-desorption isotherms of TiO_2 and Co/TiO_2 catalyst, (b) XRD patterns of TiO_2 and Co/TiO_2 catalyst after calcination and reduction, (c). TEM image of calcined Co/TiO_2 catalyst and (d). H_2-TPR profiles of TiO_2 and Co/TiO_2 catalyst.

Table 2. H_2 consumption, %Co reducibility, and acidity of TiO_2 and Co/TiO_2 catalyst.

Sample	H_2 consumption[a] (mmol g^{-1})					%Co reducibility[b]	Acidity[c] (µmol NH_3 g^{-1})			
	$Co_3O_4 \rightarrow CoO$	$CoO \rightarrow Co^0$	Reduction of $CoTiO_3$	-	Total		Weak	Medium	Strong	Total
TiO_2	-	-	-	-	-	-	29	6	4	39
Co/TiO_2	0.22	0.51	0.33	0.04	1.10	66.1	40	10	14	64

[a] Determined from H_2-TPR data. [b] Calculated from the deconvoluted area of $Co_3O_4 \rightarrow Co^0$ to the total area obtained from H_2-TPR data.[36] [c] Categorized as weak (< 200 °C), medium (200-350 °C), and strong (350-500 °C) acid sites obtained from NH_3-TPD measurement.[37]

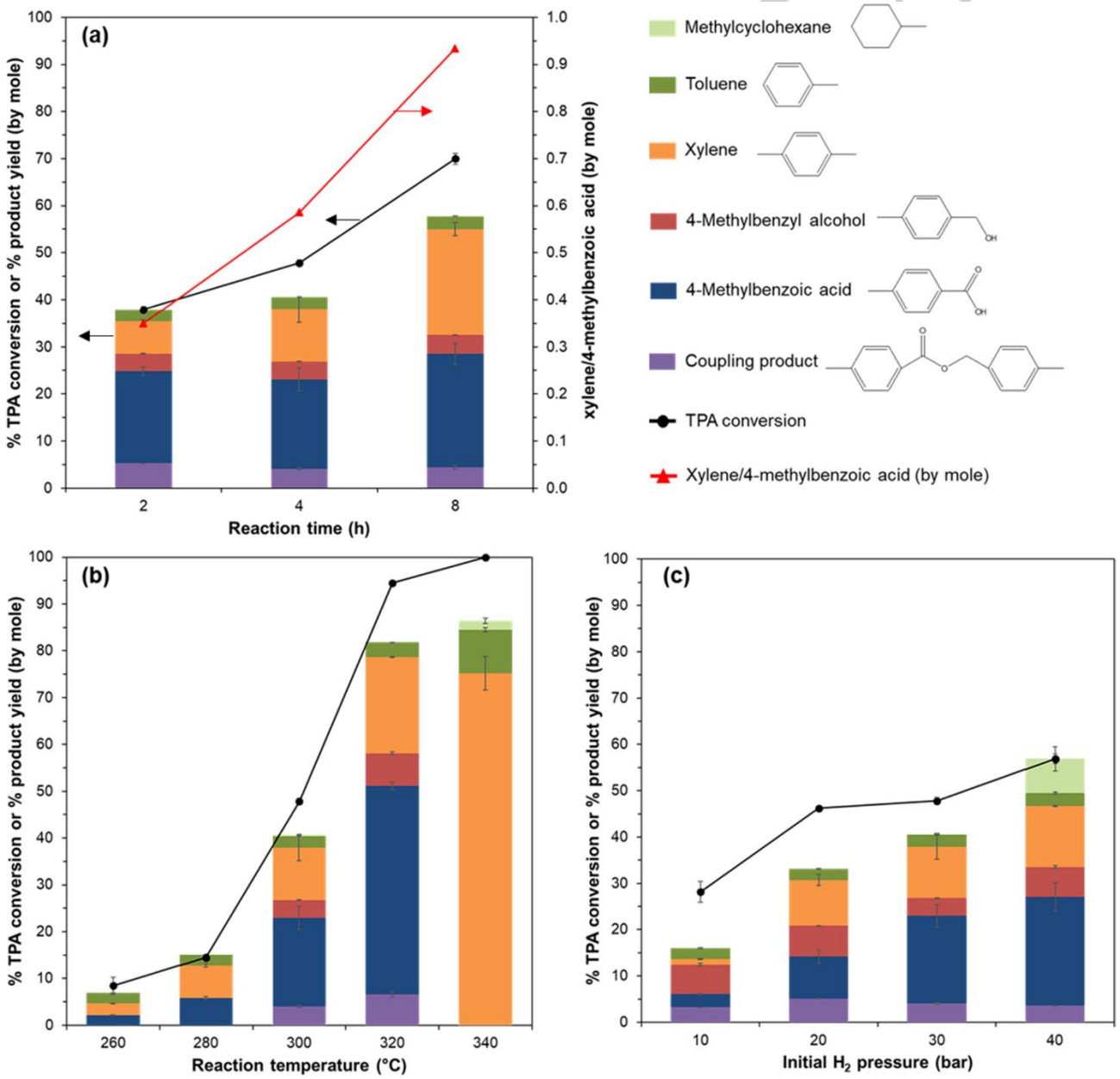

Figure 2. Effect of reaction parameters on the degree of TPA conversion and product yields obtained from HDO of TPA over Co/TiO_2 catalyst: (a) reaction time, (b) reaction temperature, and (c) initial H_2 pressure. (Central condition: 30 bar initial H_2 pressure at 300 °C for 4 h).

In order to identify the reaction pathway, the effect of reaction temperature and initial H_2 pressure on the HDO of TPA were investigated. Figure 2b exhibited the catalytic activity as a function of temperature. When the reaction was conducted at 260-280 °C and 30 bar initial H_2 pressure for 4 h, low conversion in the range of 8.5.3-14.5% was observed. The conversion sharply enhanced to 94.5-100% when the reaction temperature was increased to 320-340 °C. Not only the conversion, but also the

product selectivity was highly temperature-dependent. Increasing temperature from 300 to 320 °C dramatically enhanced the xylene and 4-methylbenzoic acid yields from 11.1 to 20.5 mol% and 18.9 to 44.4 mol%, respectively, with increasing TPA conversion from 47.8 to 94.5 mol%. These results confirm sequential conversion of TPA to 4-methylbenzoic acid and then xylene. Furthermore, the amounts of 4-methylbenzyl alcohol and a coupling product, (4-methylphenol)methyl 4-methylbenzoate, formed at 320 °C was greater than those produced at 300 °C, implying that 4-methylbenzyl alcohol may be an intermediate between 4-methylbenzoic acid and xylene. Simultaneously, 4-methylbenzoic acid or its derivatives might be coupled together to form (4-methylphenol)methyl 4-methyl benzoate. At 340 °C, 4-methylbenzoic acid and coupling products disappeared with increased formation of xylene (75.2 mol% yield). Of note, a moderate amount of toluene (9.2 mol% yield) was also detected at this reaction temperature, hinting at the presence of the 4-methylbenzoic acid decarbonylation pathway to lose one carbon. A similar phenomenon was observed by Li et al.[38] that an aldehyde intermediate (1-octadecanal) was produced during the HDO of stearic acid, which then underwent decarbonylation to heptadecane as a side product. Likewise, Izadi et al.[39] reported that the decarbonylation of 4-carboxybenzaldehyde to benzoic acid occurred during the hydrogenation of the 4-carboxybenzaldehyde to 4-(hydroxymethyl)benzoic acid. Another possibility is that the carboxylic acid undergoes decarboxylation to transform C_8 to C_7 products, which was established in a previous study over Ni based catalyst.[40]

Figure 2c showed the effect of initial H_2 pressure on the HDO of TPA. The increase in H_2 pressure from 10-40 bar promoted the TPA conversion when the reaction temperature was kept constant at 300 °C for 4 h. The TPA conversion remarkably increased from 28.1 to 46.2 mol% when the initial H_2 pressure was increased from 10 to 20 bar. Above this point, the TPA conversion continued to improve (55.2 mol% at 40 bar). Although the effect of initial H_2 pressure did not impact to the conversion of TPA as significant as the varying temperature, it drastically affected the selectivity towards arene products. It was noticed that xylene and 4-methylbenzoic acid yields were improved when a higher initial H_2 pressure was employed, correlated with the increased TPA conversion. Moreover, the HDO of TPA operated under 40 bar initial H_2 pressure afforded methylcyclohexane at 7.3 mol% yield, indicating that high H_2 pressure could promote both decarbonylation and benzene ring hydrogenation.

To confirm aldehyde was an intermediate species during TPA conversion, the HDO of 4-methylbenzaldehyde to form 4-methylbenzyl alcohol was investigated. As shown in Figure 3, close to 100% 4-methylbenzaldehyde conversion was achieved with 4-methylbenzyl alcohol (70.1 mol%) as the main product when the system was operated under 30 bar H_2 pressure at 220 °C for 15 min. Methylcyclohexane was the major side product, achieving 20.9 mol% yield. It is evident that this C_7 saturated product was produced via decarbonylation followed by hydrogenation. Considering TPA would hardly convert under this condition, 4-methylbenzaldehyde has much higher reactivity and is easily converted to 4-methylbenzyl alcohol as well as decarbonylated products. At 260 and 300 °C, the 4-methylbenzaldehyde conversion remained quantitative, while the product distribution was shifted from 4-methylbenzyl alcohol to xylene and toluene with the yields in the range of 82.1-87.9 mol% and 2.4-3.3 mol%, respectively. These results confirmed that xylene was produced from the HDO of 4-methylbenzyl alcohol. When the HDO of 4-methylbenzaldehyde was performed at 300 °C for 60 min, the formation of dimethylcyclohexane with 39.7 mol% yield via hydrogenation of xylene was obtained. The total product yield detected by GC-FID was only 51 mol%, suggesting that the higher reaction temperature and longer reaction time probably promoted hydrocracking of certain products, leading to the enhanced selectivity towards the gaseous compounds as previous reported in the literature.[41] Considering decarbonylation products, it was found that the yields of toluene and methylcyclohexane decreased from 20.9 to 2.4 mol% when the reaction temperature was increased from 220 to 260 °C with 15 min reaction time, indicating that the decarbonylation was favorable when the system was operated at low temperature, whereas the hydrogenation/hydrodeoxygenation occurred at elevated reaction temperature.

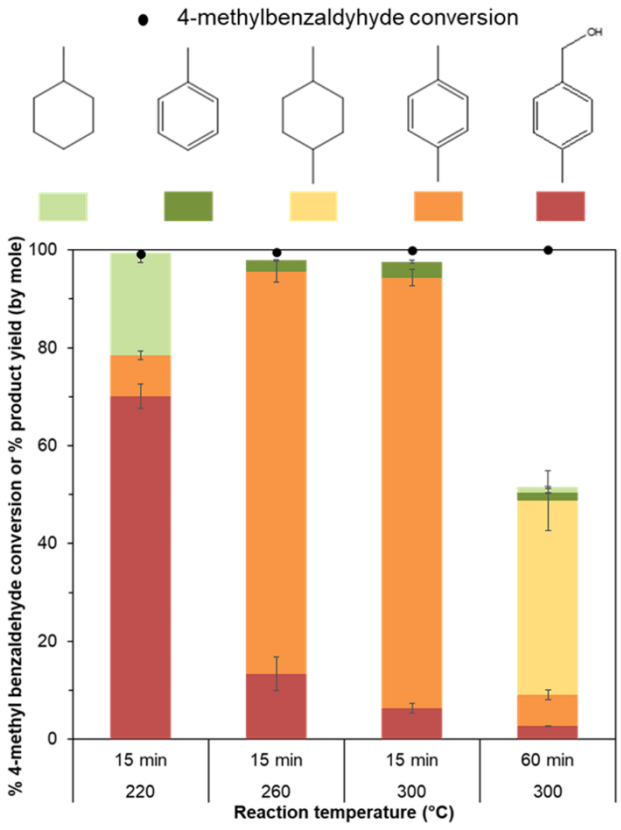

Figure 3. The degree of 4-methylbenzaldehyde conversion and product yields obtained from HDO of 4-methylbenzaldehyde over Co/TiO_2 catalyst operated under 30 bar initial H_2 pressure at 220-300 °C for 15 and 60 min.

Based on the results shown above, the reaction network for the HDO of TPA over the Co/TiO_2 catalyst was proposed in Scheme 1. According to the product distribution shown in Figure 2, 4-methylbenzoic acid and xylene were observed as the main products, while toluene and methylcyclohexane with small contents were detected as minor products. Thus, it is not unreasonable to suggest that TPA was mainly converted to 4-methylbenzoic acid via hydrodeoxygenation and hydrogenation through 4-carboxybenzaldehyde and 4-(hydroxymethyl)benzoic

acid intermediates, which could not be detected by GC-MS analysis. 4-Methylbenzoic acid was further hydrogenated and sequentially produce 4-methylbenzaldehyde, 4-methylbenzyl alcohol, xylene, and dimethylcyclohexane (**Route A**). This route is in line with the reaction pathway for TPA hydrogenation over Pd-based catalyst presented by Tourani et al.[42] Differently, the oxygenated ring-hydrogenated products (e.g., cyclohexanecarboxylic acid and cyclohexanedicarboxylic acid) found in earlier studies [39, 42] were not observed here. This might be related to the lower hydrogenation activity of the non-noble Co-based catalyst than that of the noble Pd-based ones.

In a parallel pathway (**Route B**), decarboxylation/decarbonylation occurred, leading to products bearing 7 carbons. The Co/TiO_2 catalyst with weak acidity[43] could probably promote decarboxylation of TPA or decarbonylation of 4-carboxybenzaldehyde to form benzoic acid as an intermediate, which further leads to the formation benzaldehyde, benzylalcohol, toluene, and methylcyclohexane via hydrogenation/hydrodeoxygenation. Moreover, toluene could be formed through decarboxylation of 4-methylbenzoic acid or decarbonylation of 4-methylbenzaldehyde (**Route C**). Route A ia always the major pathway while the relative extend of Route B and C depends on the reaction condition.

Hydrodeoxygenation of PET

HDO of PET has been conducted to access the effectiveness of the Co/TiO_2 catalyst in converting real plastic. The main results were shown in Figure 4 while the representative GC-MS chromatogram was presented in Figure S3. A variety of products has been identified and quantified by calibration data generated from GC-MS, as shown in Table S2 and Table S3, respectively. The products were divided into 5 groups: (1) cyclic hydrocarbons, (2) arenes without oxygen atoms, (3) alkylbenzoic acids or alkylbenzoates, (4) alkylterephthalic acids or alkylterephthalates, and (5) coupling product. Under 30 bar initial H_2 pressure at 320 °C for 4 h, the total product yield was 15.6 mol% (calculated based on the ratio between the moles of product and the mole of monomer unit of PET). This indicated that 4 h reaction time was insufficient to depolymerize the long-chain polymer. The total product yield was remarkably improved to 56.6 and 89.7 mol% for the longer reaction time to 8 h and 24 h, respectively. The main products obtained after 8 h reaction were alkylbenzoic acids, alkylbenzoates and coupling products. In contrast, high yields of arenes (78.9 mol%), in particular xylene and toluene, were observed when the reaction time was further raised to 24 h. It suggests that arenes are formed at the expenses of converting coupling products/alkylbenzoic acids/alkylbenzoates. Moreover, the increase in the total product yields for the system operated at the longer reaction from 8 to 24 suggested the presence of oligomers during the early stage of the reaction, which cannot be detected by GC and GC-MS. This is also in full agreement with observation of self-accelerated reaction kinetics of PET conversion.

According to the representative GC-MS chromatogram (Figure S3), ester compounds derived from terephthalic acid or benzoic acid, such as diethylterephthalate, ethyl 4-methylbenzoate, methyl 4-methylbenzoate, and 2-hydroxyethyl 4-methylbenzoate were observed. Based on the existence of these chemicals as intermediates, and the fact that the reaction was conducted in *n*-dodecane with negligible water content, we tentatively propose depolymerization of PET occurred via C-O bond hydrogenolysis over the Co-based catalyst.[26c] As shown in Figure S4, the PET polymer chain could be broken at two positions to produce either the benzaldehyde-end chain and hydroxyethyl benzoate-end chain species, or the benzoic-end chain and ethyl benzoate-end chain compounds. The ethyl group in the hydroxyethyl benzoate-end chain and ethyl benzoate-end chain products might be further removed via hydrogenolysis, following which the aromatic part join the reaction network as shown in Scheme 1.

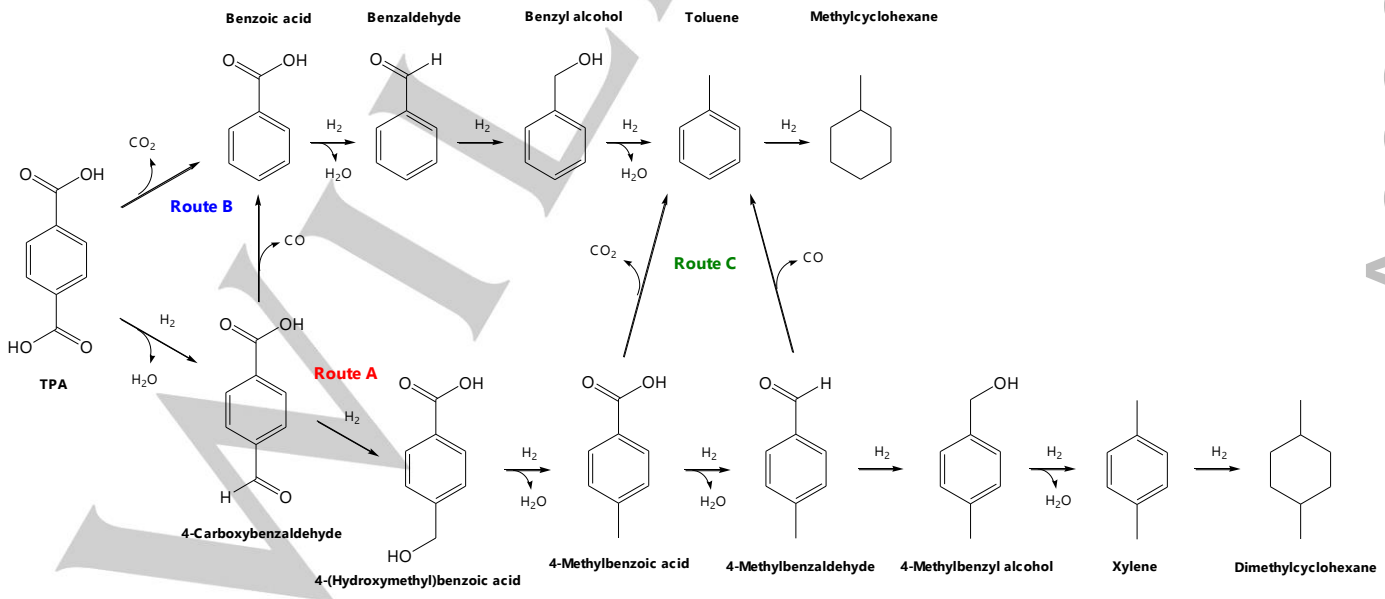

Scheme 1. Proposed reaction pathway for the HDO of TPA over Co/TiO_2 catalyst.

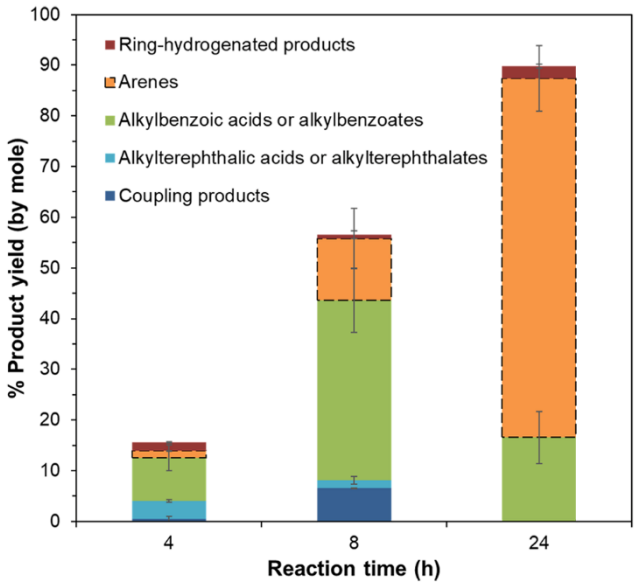

Figure 4. The degree of product yields obtained from HDO of PET resin over Co/TiO_2 catalyst under 30 bar initial H_2 pressure at 320 °C.

Ethylene glycol or its derived products was not detected in GC-MS, hinting that the ethylene glycol moiety in the ethyl benzoate-end or hydroxyethyl benzoate-end chains was converted into gaseous products. To confirm this, the gas product obtained from the HDO of PET in dodecane under 30 bar initial H_2 pressure at 320 °C for 4 h was investigated by GC-TCD. The result as summarized in Table S4 indicated the formation of CO_2, methane, ethylene, and ethane in the gas phase. By comparing with the control experiment using pure dodecane, methane is mainly derived from the solvent, while ethylene, ethane, and CO_2 were mainly obtained from HDO of PET. The results suggested that ethylene glycol part was converted to C_2 deoxygenated products, ethane and ethylene, and partially to CO_2 during the HDO process.

From above, the Co/TiO_2 catalyst is efficient in converting PET into arene compounds via C-O bond cleavage followed by HDO.[26c, 44] Several unique structural features may endow the catalyst the desired catalytic performances. First, the Co particles stay in the out shell of the support, facilitates the access of active sites by substrates. Secondly, the incorporation of Co does not only bring in metal functions for H_2 activation, but also enhanced the acidity of the material, creating a bifunctional system that is known to be beneficial for HDO of biomass in a number of earlier studies.[45] It is plausible that both weakly acidic CoO_x and TiO_x acted as role for C-O cleavage by enhancing the substrate adsorption.[26a, 26b] Finally, the strong metal-support interaction between Co and TiO_2 enhanced the stability of the catalysts.[28a] As a result, the Co catalyst remains highly active after 8 h reaction at 320 °C (as evidenced by the dramatic increase of product yield between 8-24 h reaction).

When the spent Co/TiO_2 catalyst was directly used in a second batch, the total product yield decreased from 90 mol% to 35 mol% with significant reduction of arene products (Figure 5). Attempt to regenerate the catalyst after the first run, by calcination and reduction under H_2 atmosphere, was also not successful (~20 mol% products). These results suggested that the Co/TiO2 catalyst was dramatically deactivated after 24 h of PET conversion. Figure S5 showed TGA thermogram of the spent catalyst after one batch reaction. The weight loss during 200-800 °C was 1.5 wt%. Therefore, coke formation was unlikely to be the main reason for deactivation. Next, XRD patterns of the spent catalyst from both recycle and regeneration were collected to compare with the freshly reduced catalyst (Figure S6a). The characteristic peak of anatase TiO_2 at 2θ of 25.3° was remarkably decreased with appearance of the peak at 2θ of 27°, corresponding to rutile TiO_2,[32] which is less active in HDO according to previous studies.[27b, 46] Moreover, the peak at about 44.3° attributed to the metallic Co^0 disappeared after the reaction (Figure S6b). while the new peaks at 2θ of 33° and 35°, which correspond to the (104) and (110) planes for $CoTiO_3$, appeared in the reuse and regenerated samples.[47] These indicated the loss of active metallic Co during the process. To improve the recyclability of the catalyst, identifying catalyst that operates at a milder reaction condition to prevent phase transformation of TiO_2 and Co into $CoTiO_3$ is necessary. Previous studies reported that the incorporation of Co with highly active noble metal such as Pt, Pd, and Ru,[48] provided bimetallic catalysts with the improved HDO activity in biomass conversion process. In parallel, the addition of some metal oxides such as alumina, silica, or zirconia into TiO_2 support are expected to inhibit the phase transformation of TiO_2[32] The obtained composite TiO_2-metal oxide support may also have larger area than the pure TiO_2 support.[49] These are possible future directions for catalyst design

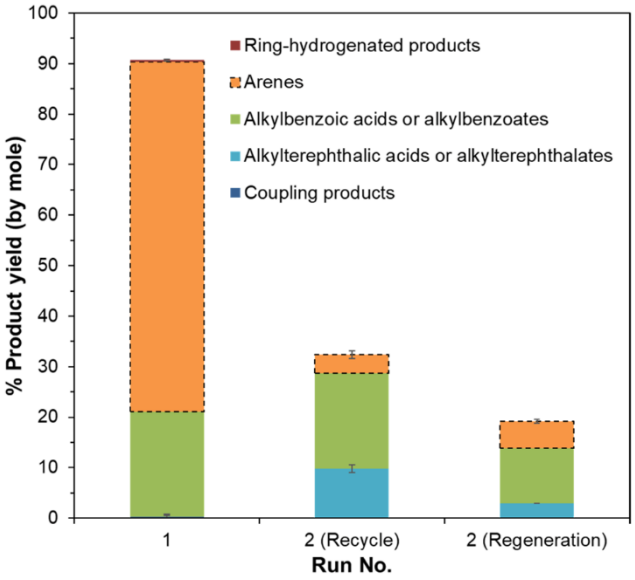

Figure 5. Ability to recycle and regeneration of Co/TiO_2 catalyst for HDO of PET operated under 30 bar initial H_2 pressure at 320 °C for 24 h.

Conclusions

In this work, a 5 wt% Co/TiO_2 catalyst was developed to convert the PET polymer back to arenes in the presence of hydrogen. The Co/TiO_2 catalyst possessed a low BET surface area with Co particles located outside the pore with weak acidity, providing direct interaction between Co and large-molecule

substrates such TPA or PET, as well as a metal-acid bifunctional system beneficial for HDO. In the conversion of PET monomer, TPA, 75.2 mol% arenes in particular xylene and toluene were achieved when the system was carried out under 30 bar initial H_2 pressure at 340 °C for 4 h. The main reaction pathway includes hydrogenation and hydrodeoxygenation, while decarboxylation/decarbonylation is the sideway towards toluene. HDO of PET resin was also conducted, and the Co/TiO_2 catalyst promoted both depolymerization and HDO of PET via C-O cleavage to produce arenes (xylene and toluene) with 78.9 mol% yield. This study identifies a 3-d metal-based catalyst and optimized reaction condition to convert PET into useful arenes, adding a new catalytic system into the toolbox for chemical upcycling of plastic waste. The major limitation of the catalyst is its insufficient stability during the reaction due to phase transformation of the TiO_2 support and the loss of metallic Co by forming $CoTiO_3$, which remains to be overcome in future works.

Experimental Section

Chemicals and materials

Terephthalic acid (TPA; 98%), p-tolualdehyde (97%), n-dodecane (anhydrous, ≥99%), n-octane (anhydrous, ≥99%), pentadecane (≥ 99%), guaiacol (99%), ethyl acetate (≥99%, HPLC), N,N-dimethylformamide (anhydrous, 99.8%), Hexamethyldisilazane (ReagentPlus, ≥99.9%), cobalt nitrate hexahydrate ($Co(NO_3)_2$•$6H_2O$), and titanium dioxide in anatase form (TiO_2; 99.8%, powder) were purchased from Sigma-Aldrich (Singapore). PET resin (grinded into powder form; < 500 µm) was obtained from Thai PET Resin Co., Ltd. All chemicals were used without purification.

Catalyst preparation

5 wt% Co/TiO_2 catalyst used in this research was prepared via the wetness impregnation method. A gram of TiO_2 powder was added into 0.05 M cobalt nitrate solution (3 mL). The mixture was stirred for 5 h at room temperature and consecutively dried in an oven at 50 °C overnight. The resulting product was then calcined at 500 °C for 3 h with a heating rate of 5 °C/min. Before catalytic testing, the calcined catalyst was *ex situ* reduced in a tubular furnace under the H_2 atmosphere at 420 °C for 2 h with a heating rate of 5 °C/min.

Catalyst characterization

The actual Co content in the Co/TiO_2 catalyst was analyzed by Inductively coupled plasma optical emission spectrometry (ICP-OES) performed by ICP Spectrometer (Thermo Scientific: iCAP 6000 series). The sample (10 mg) was digested in aqua regia (4 mL) for 3 days. The obtained mixture was diluted in DI water and its volume was adjusted to 25 mL. The remained particles were removed before analysis. Field-emission transmission electron microscope (FETEM) images of Co/TiO_2 catalyst were taken by the FETEM system of JOEL microscopy (model JEM-2100F). X-ray diffraction (XRD) patterns of TiO_2 and Co/TiO_2 catalyst were obtained using XRD analyzer (Bruker: D8 Advance). The 2θ was varied in a range of 5-80° with a step size of 0.02° and counting time of 0.4 s/step. The Co crystallite size was calculated using Scherrer's equation with the characteristic peak of Co^0 at 44.3θ obtained from XRD.[26a] The Co crystallite size (d_{Co}) was used to estimate the percentage of Co dispersion ($\%D_{Co}$) using the relation equation: $\%D_{Co} = 96/d_{Co}$ assuming spherical Co particles with site density 14.6 atom/nm.[26a] N_2 adsorption-desorption of supports and catalysts were tested using Quantachrome (NOVA touch 4LX) to evaluate specific surface area (S_{BET}), total pore volume (V_p), and pore radius (r_p). Before evaluation, the samples (50 mg) were degassed at 300 °C for 3 h to remove remaining gas in samples. The S_{BET} was calculated from adsorption data (at P/P0 ≥ 0.3), and the V_p was gained from a maximum adsorption volume (at P/P = 0.95). The r_p was estimated using Barret-Joyner-Halenda (BJH) method cumulative desorption mode. The profiles of H_2 temperature-programmed reduction (H_2-TPR) of TiO_2 and calcined Co/TiO_2 catalyst were conducted in the Belcat-Basic Chemisorption analyzer (BELCAT II). The samples were prior pretreated in Ar at flow rate of 30 ml/min at 100 °C for 0.5 h. The 5% (v/v) H_2/Ar mixed gas (30 mL/min) was then applied in the reduction measurement step. The sample cell was heated from 100 to 900 °C with a ramp rate of 10 °C/min. The degree of Co reducibility was calculated from the fraction of deconvoluted area for the reduction of Co_3O_4 (Co_3O_4 → Co^0) to total area obtained from H_2-TPR data, as described in previous study.[36] The acidity of TiO_2 and Co/TiO_2 catalyst was evaluated using temperature-programmed desorption of ammonia (NH_3-TPD) conducted by Basic Chemisorption analyzer (BELCAT II). After pretreatment under He atmosphere (flow rate = 50 mL/min) at 500 °C for 1 h and then cooling down to 40 °C, the NH_3 adsorption step was conducted using 5% NH_3/He mixed gas with a flow rate of 50 mL/min for 1 h. Then, the system was flushed by He gas at a flow rate of 50 mL/min for 1 h to remove physisorbed NH_3. The temperature of sample cell was increased to 500 °C with a heating rate of 10 °C/min to desorb NH_3. The amount of released NH_3 was detected by a thermal conductivity detector (TCD).

Hydrodeoxygenation of TPA or PET over Co/TiO_2 catalyst

Typically, HDO of TPA or PET using Co/TiO_2 catalyst was carried out in a 20 mL stainless steel autoclave. The reduced catalyst was loaded into the reactor containing TPA (300 mg), n-dodecane (4 mL) used as the solvent, and a magnetic stirrer bar. After purging the system with H_2 gas for 6 times, the system was pressurized to the desired initial H_2 pressure and heated up to the reaction temperature before starting the agitation at a constant stirring speed of 700 rpm and held for a given reaction time interval. When the reaction was ceased, the reactor was placed in a water bath to cool down the system to room temperature. The 8 mL ethyl acetate was then poured into the resulting solution to improve the solubility and dissolve some matter remaining in the liquid product.[46] Moreover, 100 µL n-octane was added as an internal standard. The solid fraction (spent catalyst and unreacted TPA) and liquid products were separated by centrifugation for 15 min. The liquid product was quantitatively analyzed using gas chromatography equipped with a flame ionization detector (GC-FID; Agilent 7890A) and HP-5 column calculated using a calibration curve. The chemical compositions in the liquid product were also identified using gas chromatography-mass spectrometry (GC-MS; Agilent 7890A). For both GC-FID and GC-MS analysis, the initial column temperature was controlled at 50 °C and then increased to 280 °C at a heating rate of 10 °C/min. In the case of TPA, according to the insolubility of TPA in dodecane and ethyl acetate, an additional procedure was required to determine the actual amount of unreacted TPA after the HDO. Typically, the unreacted TPA was extracted from the solid fraction using 4 mL N,N-dimethylformamide.[38] Hexamethyldisilazane and pentadecane were used as a derivatized agent and internal standard, respectively, to determine the amount of unreacted TPA using the similar GC-FID and GC-MS conditions.

The percentage of substrate conversion and yields of each component found in the liquid product were calculated using equations (1) and (2), respectively. The amount of each compound was evaluated by the calibration curve obtained from GC-FID spectroscopy. All calibration data were exhibited in Table S1.

$$\text{Conversion}\ (\%) = \frac{\text{Reacted substrate (mol)}}{\text{Fed substrate (mol)}} \times 100 \quad (1)$$

$$\text{Product (i) yield}\ (\%) = \frac{\text{Amount of product (i) (mol)}}{\text{Fed substrate (mol)}} \times 100 \quad (2)$$

For the HDO of PET resin, the chemical components in the liquid product were qualitatively and quantitatively examined by GC-MS (Shimazu-2010, equipped with HP-5 column) using guaiacol as an internal standard to calculate the amount of each product species. The yield of each composition in the obtained liquid product was quantified by using calibration data prepared by GC-MS spectroscopy, as shown in Table S3. Xylene, benzoic acid, dimethylterephthlate, and benzylbutyl phthalate

were selected as representative chemicals in each product groups to generate calibration curve from GC-MS. Xylene calibration curve was used to calculate the amounts of product without oxygen atom (ring-hydrogenated products and arenes). While, the calibration data of benzoic acid, dimethylterephthalate, and benzylbutyl phthalate were applied to quantify the amount of products in groups of alkylbenzoic acids or alkylbenzoates, alkylterephthalic acids or alkylterephthalates, and coupling products, respectively.

To investigate the catalyst recyclability, the Co/TiO_2 catalyst obtained from the HDO of PET under 30 bar initial H_2 pressure at 320 °C for 24 h was directly recycled to conduct the HDO of PET under the same reaction condition. To investigate whether the catalyst could be readily regenerated, the spent Co/TiO_2 catalyst obtained from HDO of PET was treated by calcination and reduction under H_2 atmosphere again by using the method for preparation of the fresh Co/TiO_2 catalyst before conducting a second batch HDO reaction.

Acknowledgements

The authors gratefully acknowledge the financial support from NUS Flagship Green Energy Program (R-279-000-553-646, and R-279-000-553-731) and Thailand Research Fund and National Research Council of Thailand for providing a Royal Golden Jubilee Ph.D. Program (Grant No. PHD/0014/2561).

Keywords: Hydrodeoxygenation • Polyethylene terephthalate • Terephthalic acid • Cobalt • Titanium dioxide

[1] Y. Xue, P. Johnston, X. Bai, *Energy Convers. Manage.* **2017**, *142*, 441-451.

[2] a) S. Bezergianni, A. Dimitriadis, G.-C. Faussone, D. Karonis, *Energies* **2017**, *10*, 1750; b) PlasticsEurope, "Plastics-The Facts 2020: An analysis of European plastics production, demand and waste data". Available from https://www.plasticseurope.org/en/resources/publications/4312-plastics-facts-2020 (accessed June 2021).

[3] a) M. Yudell, D. Roberts, R. DeSalle, S. Tishkoff, *Science* **2020**, *369*, 1313; b) K. R. Vanapalli, H. B. Sharma, V. P. Ranjan, B. Samal, J. Bhattacharya, B. K. Dubey, S. Goel, *Sci. Total Environ.* **2021**, *750*, 141514.

[4] a) J. M. Garcia, M. L. Robertson, *Science* **2017**, *358*, 870-872; b) R. Geyer, J. R. Jambeck, K. L. Law, *Sci. Adv.* **2017**, *3*, e1700782; c) J. R. Jambeck, R. Geyer, C. Wilcox, T. R. Siegler, M. Perryman, A. Andrady, R. Narayan, K. L. Law, *Science* **2015**, *347*, 768-771; d) K. L. Law, N. Starr, T. R. Siegler, J. R. Jambeck, N. J. Mallos, G. H. Leonard, *Sci. Adv.* **2020**, *6*, eabd0288.

[5] K. Li, S. Lee, G. Yuan, J. Lei, S. Lin, P. Weerachanchai, Y. Yang, J.-Y. Wang, *Energies* **2016**, *9*.

[6] Z. Guo, N. Yan, A. A. Lapkin, *Curr. Opin. Chem. Eng.* **2019**, *26*, 148-156.

[7] D. Munir, M. F. Irfan, M. R. Usman, *Renewable Sustainable Energy Rev.* **2018**, *90*, 490-515.

[8] A. M. da Costa, V. R. de Oliveira Lopes, L. Vidal, J.-M. Nicaud, A. M. de Castro, M. A. Z. Coelho, *Process Biochem.* **2020**, *95*, 81-90.

[9] a) J. Chu, Y. Cai, C. Li, X. Wang, Q. Liu, M. He, *Waste Manage.* **2021**, *124*, 273-282; b) R. Zhang, X. Ma, X. Shen, Y. Zhai, T. Zhang, C. Ji, J. Hong, *J. Environ. Manage.* **2020**, *260*, 110062; c) A. Rahimi, J. M. García, *Nat. Rev. Chem.* **2017**, *1*.

[10] V. Sinha, M. R. Patel, J. V. Patel, *J. Polym. Environ.* **2008**, *18*, 8-25.

[11] a) K. Ikenaga, T. Inoue, K. Kusakabe, *Procedia Eng.* **2016**, *148*, 314-318; b) H. L. Lee, C. W. Chiu, T. Lee, *Chem. Eng. J. Adv.* **2021**, *5*, 100079.

[12] Y. Liu, X. Yao, H. Yao, Q. Zhou, J. Xin, X. Lu, S. Zhang, *Green Chem.* **2020**, *22*, 3122-3131.

[13] F. Liu, J. Chen, Z. Li, P. Ni, Y. Ji, Q. Meng, *J. Anal. Appl. Pyrolysis* **2013**, *99*, 16-22.

[14] a) B. F. S. Nunes, M. C. Oliveira, A. C. Fernandes, *Green Chem.* **2020**, *22*, 2419-2425; b) Y. Kratish, J. Li, S. Liu, Y. Gao, T. J. Marks, *Angew. Chem. Int. Ed.* **2020**, *59*, 19857-19861; *Angew. Chem.* **2020**, *132*, 20029-20033.

[15] a) B. Geyer, G. Lorenz, A. Kandelbauer, *eXPRESS Polym. Lett.* **2016**, *10*, 559-586; b) A. M. Al-Sabagh, F. Z. Yehia, G. Eshaq, A. M. Rabie, A. E. ElMetwally, *Egypt. J. Pet.* **2016**, *25*, 53-64.

[16] R. Miandad, M. Rehan, M. A. Barakat, A. S. Aburiazaiza, H. Khan, I. M. I. Ismail, J. Dhavamani, J. Gardy, A. Hassanpour, A.-S. Nizami, *Front. Energy Res.* **2019**, *7*.

[17] a) M. Sogancioglu, G. Ahmetli, E. Yel, *Energy Procedia* **2017**, *118*, 221-226; b) O. J. Odejobi, A. A. Oladunni, J. A. Sonibare, I. O. Abegunrin, *Fuel Commun.* **2020**, *2-5*.

[18] a) A. C. Fernandes, *ChemSusChem* **2021**, DOI: 10.1002/cssc.202100130; b) S. Lu, Y. Jing, B. Feng, Y. Guo, X. Liu, Y. Wang, *ChemSusChem* **2021**, DOI: 10.1002/cssc.202100196; c) X. Chen, Y. Wang, L. Zhang, *ChemSusChem* **2021**, DOI: 10.1002/cssc.202100868.

[19] H. Tang, N. Li, G. Li, A. Wang, Y. Cong, G. Xu, X. Wang, T. Zhang, *Green Chem.* **2019**, *21*, 2709-2719.

[20] H. Tang, Y. Hu, G. Li, A. Wang, G. Xu, C. Yu, X. Wang, T. Zhang, N. Li, *Green Chem.* **2019**, *21*, 3789-3795.

[21] Y. Jing, Y. Wang, S. Furukawa, J. Xia, C. Sun, M. J. Hulsey, H. Wang, Y. Guo, X. Liu, N. Yan, *Angew. Chem. Int. Ed.* **2021**, *60*, 5527-5535; *Angew. Chem.* **2021**, *133*, 5587-5595.

[22] a) S. S. Wong, R. Shu, J. Zhang, H. Liu, N. Yan, *Chem. Soc. Rev.* **2020**, *49*, 5510-5560; b) X. Wang, M. Arai, Q. Wu, C. Zhang, F. Zhao, *Green Chem.* **2020**, *22*, 8140-8168.

[23] a) R. Shu, B. Lin, C. Wang, J. Zhang, Z. Cheng, Y. Chen, *Fuel* **2019**, *239*, 1083-1090; b) C. Zhao, J. A. Lercher, *ChemCatChem* **2012**, *4*, 64-68; c) T. Omotoso, S. Boonyasuwat, S. P. Crossley, *Green Chem.* **2014**, *16*, 645-652; d) R. Shu, B. Lin, J. Zhang, C. Wang, Z. Yang, Y. Chen, *Fuel Process. Technol.* **2019**, *184*, 12-18.

[24] a) S. Mukundan, M. A. Wahab, L. Atanda, M. Konarova, J. Beltramini, *RSC Adv.* **2019**, *9*, 17194-17202; b) X. Lan, E. J. M. Hensen, T. Weber, *Appl. Catal. A* **2018**, *550*, 57-66; c) X. Ouyang, X. Huang, M. D. Boot, E. J. M. Hensen, *ChemSusChem* **2020**, *13*, 1705-1709; d) X. Liu, L. Xu, G. Xu, W. Jia, Y. Ma, Y. Zhang, *ACS Catal.* **2016**, *6*, 7611-7620.

[25] a) M. Lu, Y. Jiang, Y. Sun, P. Zhang, J. Zhu, M. Li, Y. Shan, J. Shen, C. Song, *Energy Fuels* **2020**, *34*, 4685-4692; b) J. Zhang, B. Fidalgo, S. Wagland, D. Shen, X. Zhang, S. Gu, *Fuel* **2019**, *238*, 257-266; c) D. Raikwar, M. Munagala, S. Majumdar, D. Shee, *Catal Today* **2019**, *325*, 117-130; d) X. Zhang, P. Yan, B. Zhao, K. Liu, M. C. Kung, H. H. Kung, S. Chen, Z. C. Zhang, *ACS Catal.* **2019**, *9*, 3551-3563; e) S. Bulut, S. Siankevich, A. P. van Muyden, D. T. L. Alexander, G. Savoglidis, J. Zhang, V. Hatzimanikatis, N. Yan, P. J. Dyson, *Chem. Sci.* **2018**, *9*, 5530-5535.

[26] a) I. T. Ghampson, C. Sepúlveda, A. B. Dongil, G. Pecchi, R. García, J. L. G. Fierro, N. Escalona, *Catal. Sci. Technol.* **2016**, *6*, 7289-7306; b) X. Liu, W. Jia, G. Xu, Y. Zhang, Y. Fu, *ACS Sustainable Chem. Eng.* **2017**, *5*, 8594-8601; c) N. T. T. Tran, Y. Uemura, A. Ramli, *Procedia Eng.* **2016**, *148*, 1252-1258.

[27] a) F. Héroguel, X. T. Nguyen, J. S. Luterbacher, *ACS Sustainable Chem. Eng.* **2019**, *7*, 16952-16958; b) M. Lu, H. Du, B. Wei, J. Zhu, M. Li, Y. Shan, C. Song, *Energy Fuels* **2017**, *31*, 10858-10865.

[28] a) Y. X. Yang, J. S. Hao, G. Q. Lv, *Fuel* **2019**, *253*, 630-636; b) L. E. Oi, M.-Y. Choo, H. V. Lee, H. C. Ong, S. B. A. Hamid, J. C. Juan, *RSC Adv.* **2016**, *6*, 108741-108754.

[29] K. A. Cychosz, R. Guillet-Nicolas, J. Garcia-Martinez, M. Thommes, *Chem. Soc. Rev.* **2017**, *46*, 389-414.

[30] H. Gai, H. Wang, L. Liu, B. Feng, M. Xiao, Y. Tang, X. Qu, H. Song, T. Huang, *Chem. Phys. Lett.* **2021**, *767*.

[31] L. J. Cardenas Flechas, A. M. Raba Paéz, M. Rincon Joya, *Dyna* **2020**, *87*, 184-191.
[32] D. A. H. Hanaor, C. C. Sorrell, *J. Mater. Sci.* **2010**, *46*, 855-874.
[33] N. Prasongthum, R. Xiao, H. Zhang, N. Tsubaki, P. Natewong, P. Reubroycharoen, *Fuel Process. Technol.* **2017**, *160*, 185-195.
[34] R. Morales, F. J. Tavera, R. E. Aune, S. Seetharaman, *Scand. J. Metall.* **2005**, *34*, 108-115.
[35] H. Azzi, I. Rekkab-Hammoumraoui, L. Chérif-Aouali, A. Choukchou-Braham, *Bull. Chem. React. Eng. Catal.* **2019**, *14*, 112-123.
[36] O. J. Olusola, M. Sudip, *J. Pet. Technol. Altern. Fuels* **2016**, *7*, 1-12.
[37] P. Sangnikul, C. Phanpa, R. Xiao, H. Zhang, P. Reubroycharoen, P. Kuchonthara, T. Vitidsant, A. Pattiya, N. Hinchiranan, *Appl. Catal. A* **2019**, *574*, 151-160.
[38] J. Li, J. Zhang, S. Wang, G. Xu, H. Wang, D. G. Vlachos, *ACS Catal.* **2019**, *9*, 1564-1577.
[39] N. Izadi, A. M. Rashidi, A. Izadi, S. Emami, V. Samimi, H. Varmazyar, *Int. J. Hydrogen Energy* **2017**, *42*, 2970-2983.
[40] W. Li, Y. Gao, S. Yao, D. Ma, N. Yan, *Green Chem.* **2015**, *17*, 4198-4205.
[41] M. Anand, S. A. Farooqui, R. Kumar, R. Joshi, R. Kumar, M. G. Sibi, H. Singh, A. K. Sinha, *Fuel Process. Technol.* **2016**, *151*, 50-58.
[42] S. Tourani, A. A. Safekordi, M. Rashidzadeh, A. M. Rashidi, F. Khorasheh, *Chem. Eng. Res. Des.* **2016**, *109*, 41-52.
[43] a) D. García-Pérez, M. C. Alvarez-Galvan, M. C. Capel-Sanchez, G. Blanco-Brieva, S. Morales-delaRosa, J. M. Campos-Martin, J. L. G. Fierro, *Catal. Today* **2021**, *367*, 43-50; b) Z. Ding, T. Zhao, Q. Zhu, S. Liao, L. Ning, Y. Bi, H. Chen, *Biomass Bioenergy* **2020**, *143*, 105879.
[44] N. M. Eagan, J. P. Chada, A. M. Wittrig, J. S. Buchanan, J. A. Dumesic, G. W. Huber, *Joule* **2017**, *1*, 178-199.
[45] a) Y. Takeda, M. Tamura, Y. Nakagawa, K. Okumura, K. Tomishige, *ACS Catal.* **2015**, *5*, 7034-7047; b) A. M. Robinson, J. E. Hensley, J. W. Medlin, *ACS Catal.* **2016**, *6*, 5026-5043; c) G. Wu, N. Zhang, W. Dai, N. Guan, L. Li, *ChemSusChem* **2018**, *11*, 2179-2188; d) N. Yan, S. Ding, *Trends Chem.* **2019**, *1*, 457-458; e) J. Zhong, J. Pérez-Ramírez, N. Yan, *Green Chem.* **2021**, *23*, 18-36.
[46] J. Mao, J. Zhou, Z. Xia, Z. Wang, Z. Xu, W. Xu, P. Yan, K. Liu, X. Guo, Z. C. Zhang, *ACS Catal.* **2016**, *7*, 695-705.
[47] a) A. Abedini, S. Khademolhoseini, *J. Mater. Sci. Mater. Electron.* **2015**, *27*, 330-334; b) M. Enhessari, S. Moqhadam, M. Kargarrazi, S. Ghezelbashi, M. Tootkani, *Int. J. Nano Dimens.* **2010**, *1*, 125-132.
[48] a) P. T. M. Do, A. J. Foster, J. Chen, R. F. Lobo, *Green Chem.* **2012**, *14*, 1388; b) N. T. T. Tran, Y. Uemura, A. Ramli, T. H. Trinh, *Mol. Catal.* **2021**, DOI: 10.1016/j.mcat.2021.111435; c) R. Shu, R. Li, Y. Liu, C. Wang, P.-F. Liu, Y. Chen, *Chem. Eng. Sci.* **2020**, *227*, 115920.
[49] X. Y. Ooi, L. E. Oi, M.-Y. Choo, H. C. Ong, H. V. Lee, P. L. Show, Y.-C. Lin, J. C. Juan, *Fuel Process. Technol.* **2019**, *194*.

1

WILEY-VCH

FULL PAPER

Entry for the Table of Contents

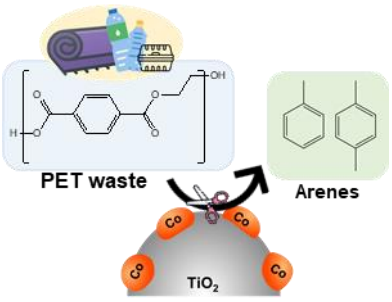

Transformation of PET over a Co/TiO_2 catalyst in the presence of hydrogen into arenes in up to 79% yield was demonstrated, thereby providing an alternative route for PET waste recycling via hydrodeoxygenation using a cheap metal based catalyst.